

# Energy Management of Multi-component Power Harvesting Systems

Robert B. MacCurdy<sup>\*a</sup>, Timothy Reissman<sup>a</sup>, Ephraim Garcia<sup>a</sup>

<sup>a</sup>Sibley School of Mechanical and Aerospace Engineering, Cornell University Laboratory for Intelligent Machine Systems, Ithaca, New York 14853

## ABSTRACT

Recent efforts in power harvesting systems have concentrated primarily on the optimization of isolated energy conversion techniques, such as piezoelectric, electromagnetic, solar, or thermal generators, but have focused less on combining different energy transducer types and have placed less emphasis on storing the converted energy for use by other devices. The purpose of this work is to analyze and present an integrated piezoelectric and electromagnetic power harvesting system utilizing existing technology for energy management and storage. Primary emphasis is on the analysis of the combination of existing, or readily obtainable, energy conversion techniques, operating as a single system, and the energy conversion efficiency of the alternating to direct current management, or storage, circuit.

**Keywords:** Power harvesting, energy harvesting, piezoelectric, electromagnetic induction, management circuitry, AC-DC efficiency, energy storage, full-wave rectification

## 1. INTRODUCTION

Research publications on power harvesting devices have seen a sharp increase within the last ten years due to the advancements in low-power electronics, specifically wireless technologies, and the corresponding limited performance growth in standard batteries. With these new embedded power source technologies, researchers have turned their focus on renewable power systems for electrical energy storage, which is the impetus for development of ambient energy transducers, also known as energy harvesters, power harvesters, or simply, generators. Researchers such as Sodano et al. [1], Glynne-Jones et al. [2], Fleurial et al. [3], and Raghunathan et al. [4] have therefore been driven to explore the available energy present for their power harvesters to utilize, where options range in the form of vibration energy, thermal-gradient energy, solar energy, amongst others. With many of these devices being ultimately integrated into printed circuit board designs, investigators such as Roundy et al. [5] and Mateu and Moll [6] have also studied scaling issues with regard to dimensions available for the power harvesting device, its mass constraints, and the minimum power generation required for it to be useful. Typically, results have shown that with limited efficiencies, as shown by Goldfarb and Jones [7] and Reissman et al. [8], for these energy transducers and the coupling of the small amounts of energy available for conversion, shown by Pereyima [9], integrated power harvesting devices are appropriate for providing low power. This has caused researchers to shift focus from the power harvester to optimizing the power transfer to the energy storage device, be it a capacitor or rechargeable battery. Approaches by researchers such as Guyomar et al. [10], Ottman et al. [11], and Shu et al. [12] have primarily concerned themselves with only piezoelectric power harvesting devices, which convert vibration energy into electrical energy. The reason that the majority of energy management circuitry is based on piezoelectric sources is that there exist a multitude of ways in which conditioning of the electrical signal generated can be performed, using characteristics such as large output voltages, high energy densities, etc. In circumstances where tuning of the piezoelectric is necessary in order to lower its resonance frequency to that of the driving frequency, many designers choose to simply add a tip mass to the cantilever's free end, see Roundy and Wright [13]. This mass is effectively a dead mass in the system, which is not practical in systems with mass limitations. An example of such a mass-limiting system would be tracking devices attached to migratory birds. With too much payload, the birds are unable to fly. Thus, a piezoelectric system can only add mass within the limits defined by the system.

---

\* [rbm7@cornell.edu](mailto:rbm7@cornell.edu); phone 1 607 255-5457; fax 1 607 255-1222

An alternative would be to use an electromagnetic induction harvester as the tip mass of the system. This extra harvester would utilize the relative motion of the piezoelectric harvester's free end with respect to the motion of the printed circuit board, which is attached to the vibrating structure. Hence, the design would allow the resonance of the piezoelectric to approach that of the driving frequency, and the mass utilized would generate power by means of the relative motion of the cantilever's tip to the vibrating structure, inducing an electromotive force in the form of an output voltage. A comparative study by Poulin et al. [14] indicates that both piezoelectric and electromagnetic systems are capable of transferring convertible amounts of energy into energy management circuitry.

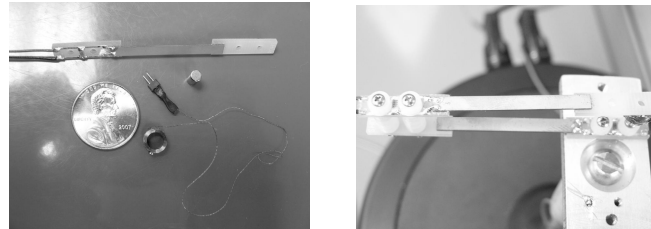


Figure 1. P-E Scale Reference of System Components and P-E System Under Investigation (from left to right)

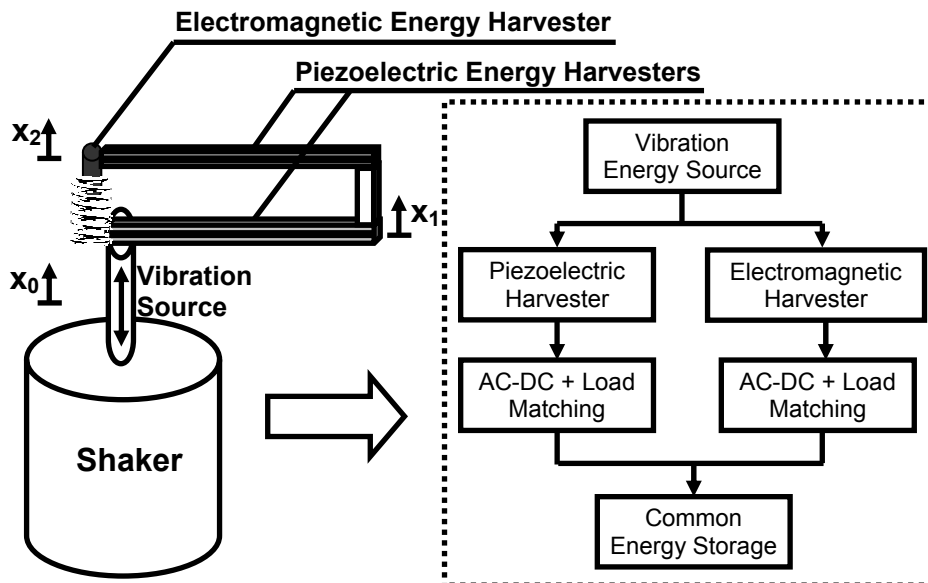


Figure 2. P-E Harvester System Schematic

The grouping together of piezoelectric and electromagnetic devices offers a superpositioning of the performance of both of these power harvesting devices originating from a single vibration energy source. Conceptually, the tuning of the piezoelectric-electromagnetic (P-E) system is performed by selection of the geometry of the individual harvesters and the total system configuration with respect to the vibration source energy. After tuning the system for maximum mechanical to electrical energy transfer, each harvester is then conditioned by an AC-DC full-wave rectifier, where the output enters into a capacitor, or load matching element. Once the DC signal for each harvester has been optimized for power efficiency, the converted energy harvesters are summed together to converge into one common energy storage element for use by the load system. Hence, a system is created in which all the components of the P-E system are used for maximizing the power, and thus the system's total power density, or efficiency, is also maximized.

## 2. P-E SYSTEM ELECTRO-MECHANICAL DYNAMICS MODEL

The P-E system can be modeled as a damped multi-degree of freedom system with a harmonic force applied to the mass of the structure which the harvesters are attached to, i.e. the vibration source, see Figure (2).

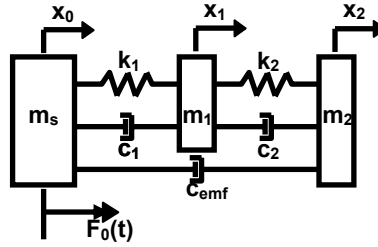


Figure 3. P-E System Dynamics Model

The parameters within the model are as follows:  $m_s$  is the mass of the vibrating structure, which is free to move in the case of a harvesting system placed on a freely moving structure, such as a flying bird. In the case of a fixed structure, as shown in Figure (1), simply connecting the mass  $m_s$  to a spring attached to a fixed frame will allow the model to conform to a conventional base excitation model. Mass  $m_1$  represents the piezoelectric energy harvester attached to the vibrating structure,  $m_s$ . Mass  $m_1$ 's coordinate  $x_1$  is with respect to the deflection of the piezoelectric energy harvester.  $k_1$  and  $c_1$  represent the stiffness and damping, mechanical and electrical, of the piezoelectric element,  $m_1$ . Likewise for the second piezoelectric harvester attached to the  $m_1$  piezoelectric harvester,  $k_2$  and  $c_2$  represent the stiffness and damping, mechanical and electrical, for the second piezoelectric harvester. The mass  $m_2$  represents the second piezoelectric which also includes the magnet's mass attached to the second piezoelectric harvester's free end, which coincides with the location of coordinate  $x_2$ . The block between the two piezoelectric harvesters is modeled as an ideal interconnect, see Khattak et al. [15].  $c_{emf}$  represents the electrical damping generated by the induced electromotive force, which is a function of the velocity of the relative motion between the electromagnetic harvester's coil and magnet. The coil is attached to  $m_s$ , and the magnet, is attached to the second piezoelectric harvester's free end, located at  $x_2$ .

Performing a free body analysis for each of the masses in the model as shown in Figure 3., the equations of motion in matrix form are shown below,

$$\begin{bmatrix} m_s & 0 & 0 \\ 0 & m_1 & 0 \\ 0 & 0 & m_2 \end{bmatrix} \ddot{x} + \begin{bmatrix} (c_1 + c_{emf}) & -c_1 & -c_{emf} \\ -c_1 & (c_1 + c_2) & -c_2 \\ -c_{emf} & -c_2 & (c_2 + c_{emf}) \end{bmatrix} \dot{x} + \begin{bmatrix} k_1 & -k_1 & 0 \\ -k_1 & (k_1 + k_2) & -k_2 \\ 0 & -k_2 & k_2 \end{bmatrix} x = \begin{bmatrix} 1 & 0 & 0 \\ 0 & 0 & 0 \\ 0 & 0 & 0 \end{bmatrix} \begin{bmatrix} F_0 \\ 0 \\ 0 \end{bmatrix} \quad (1)$$

which can be simplified to,

$$M\ddot{x} + C\dot{x} + Kx = BF(t) \quad (2)$$

where the matrices are placed in the form of a mass matrix  $M$ , a damping matrix  $C$ , a stiffness matrix  $K$ , a forcing matrix  $B$ , the forcing function vector  $F$ , and the state vector  $x$ . Using the modal analysis technique, these same equations can be manipulated into the following decoupled modal equations by letting  $x(t)=M^{1/2}q(t)$  and then letting  $q(t)=Pr(t)$ , where  $P$  is the matrix of normalized eigenvectors.

$$\ddot{r}_i(t) + 2\zeta_i\omega_i\dot{r}_i(t) + \omega_i^2r_i(t) = f_i(t) \quad (3)$$

In the case of this simple harmonic oscillator model, the solution is of the form,

$$r_{i,p}(t) = \frac{f_i}{\sqrt{(\omega_i^2 - \omega^2)^2 + (2\zeta_i\omega_i\omega)^2}} \cos(\omega t - \tan^{-1} \frac{2\zeta_i\omega_i\omega}{\omega_i^2 - \omega^2}) \quad (4)$$

where the  $r_{i,p}$  is the notation for the  $i$ th modal equation's particular solution. Evaluating the steady state solution in the physical coordinate system is carried out by the performing the transformation shown in Equation (5).

$$x_{ss}(t) = M^{-1/2} Pr(t) \quad (5)$$

Using the results of the modal analysis, a Bode plot is generated of the system as shown below in Figure (4).

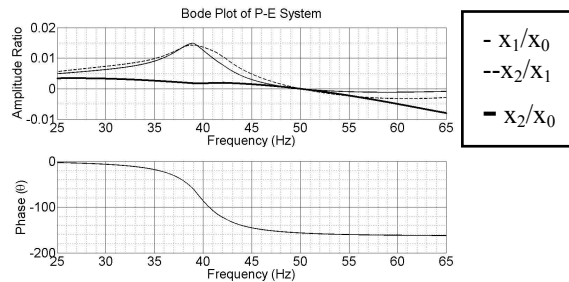


Figure 4. Amplitude Ratios and Phases Near the 1<sup>st</sup> Natural Frequency

Evaluation of the eigenvalues and eigenvectors of the equations of motion indicate the first natural frequency occurs at 40Hz. At this frequency, the mode shape indicates that the masses move in phase with one another, with varying amplitudes for each of the masses. Evaluation of the second natural frequency's mode shape indicates a 180° phase shift of the piezoelectric harvesters.

Simple power harvesting systems with one harvesting element and one or two degrees of freedom usually will not require a careful treatment of phase. This is not to say that resonances or other points of rapid transition should be ignored in the mechanical design, but the electrical output phase of a solitary harvesting element is less important because the single phase signal becomes its own reference and is immediately rectified. Rectification primarily removes the time-varying periodic component from the source. However, multi-body systems, with many coupled degrees of freedom, offer an attractive opportunity for power harvesting, because they present many locations where differential mechanical signals can be converted into useful energy. The challenge will be in exploiting these opportunities efficiently. One possible strategy already exists, and that is to simply duplicate the chain, from rectification to intermediate storage to DC/DC conversion to final power storage for each power source. The only shared component is the final storage element. This is the model that is detailed in Figure (2). It is a brute-force approach, but it decouples the harvesters from each other, which eases analysis and can make the system more uniform in frequency and phase response. The disadvantage of this approach is its complex implementation and the potential for reductions in efficiency. If harvesters are to be directly coupled, or coupled closer to the source than in Figure (2), the complete electro-mechanical system's response must be well understood.

### 3. PIEZOELECTRIC AND ELECTROMAGNETIC ELECTRICAL MODELS

Evaluation of this multi-component system is done by an analysis of each of the two separate source types. The first type utilizes the physics characterizing a piezoelectric bimorph cantilever. The piezoelectric bimorph is a cantilever beam consisting of two outer layers of piezoelectric material and an inner layer of shim material. This configuration allows for a doubling of the output of the system, compared to a unimorph, due to at least one piezoelectric layer always being in a compression state during bending. Typically, piezoelectric systems can be simplified to a model of an alternating current (AC) source with a capacitance in parallel, otherwise known as Norton equivalent circuit, see Shu and Lien [16]. Using a Thevenin equivalent model of the piezoelectric system, the equivalent circuit is shown in Figure (5), where  $C_p$  is the capacitance of the piezoelectric and the variable voltage source is a function of the vibration source, see Sodano et al [17].

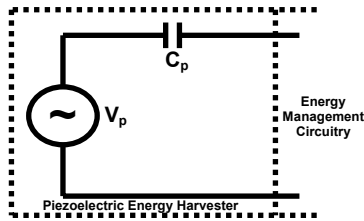


Figure 5. Piezoelectric System Electrical Circuit Equivalent

Placing the above model into a circuit analysis simulator, PSpice, plots of the performance of the piezoelectric harvester are generated using parameters obtained from open circuit testing results and compared with experimental results from variable resistive load testing of the actual P-E system, as configured in Figure (1). The capacitance of the piezoelectric harvester was measured using a B&K Precision LCR meter and entered into the model. The open circuit voltage output was entered into the model as the peak amplitude of the piezoelectric harvester and was measured by connecting the piezoelectric harvester's output leads to a high impedance oscilloscope under a prescribed base excitation acceleration and frequency, which matched the first resonance frequency of the P-E system. The driving frequency and acceleration of the base excitation, representing the vibration source, were held constant and measured using a PCB accelerometer. The following parameters shown in Figure (6) represent the simulation model. The results of the simulation are shown with comparison to experimental results in Figure (7).

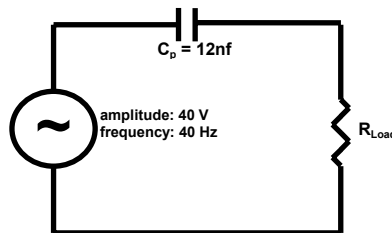


Figure 6. Piezoelectric Simulation Model Parameters

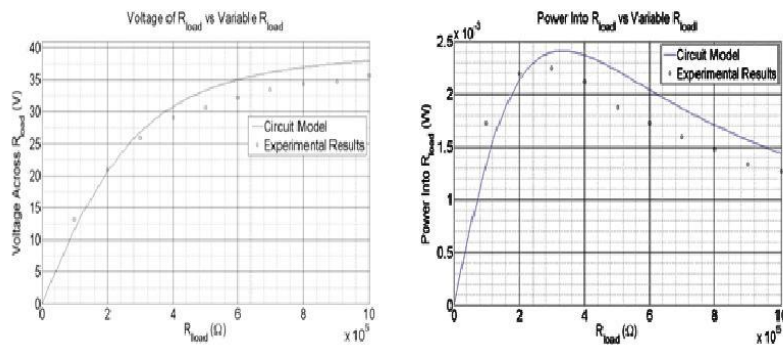


Figure 7. Piezoelectric Harvester: Voltage Across  $R_{Load}$  and Power Into  $R_{Load}$

For the electromagnetic harvester, a coil of wire is placed in a magnetic field induced by a rare-earth magnet. The change in the magnetic flux density due to the relative motion of the coil with respect to the magnet induces a voltage. This electromotive force enters into a Thevenin equivalent electrical model as a varying voltage source. The geometry of the coil is modeled as an inductive element within the circuit, while the length and diameter of the wire used to create the coil require a resistance within the circuit model. The resulting electrical circuit modeling the electromagnetic system is shown in Figure (8).

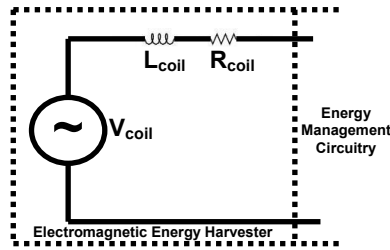


Figure 8. Electromagnetic System Electrical Circuit Equivalent

Placing the above model into the same PSpice simulator, similar plots are generated describing the electromagnetic harvester's performance. Values for the inductance and resistance are based on calculations of a coil capable of producing a 6V electromotive force voltage amplitude induced by a 1mm amplitude vibration driven at the first resonance of the P-E system. Methods used to perform these calculations are described by Greenhouse [18] and Reissman et al. [19].

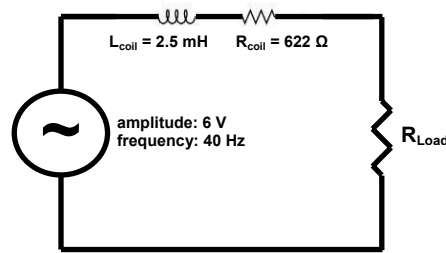


Figure 9. Electromagnetic Simulation Model Parameters

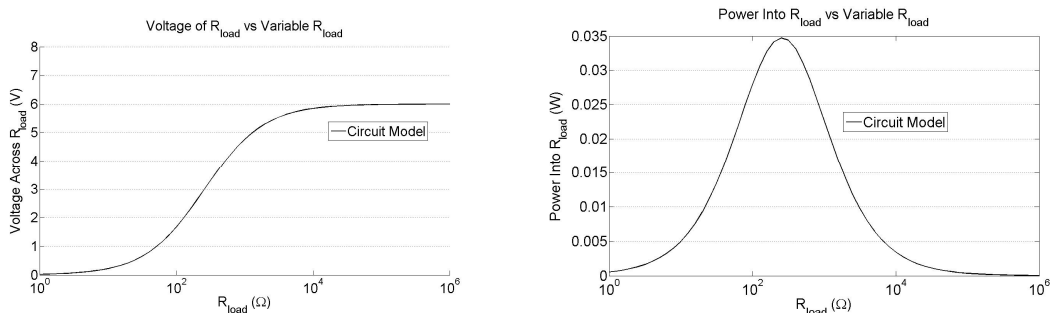


Figure 10. Electromagnetic Harvester: Voltage Across  $R_{Load}$  and Power Into  $R_{Load}$

#### 4. AC-DC CONVERSION VIA DUAL FULL-WAVE RECTIFICATION (FWR)

The piezoelectric and electromagnetic generators produce time-varying power, which must be rectified to DC for the harvested electrical energy to be useful as a power source. Two common methods to achieve this are the half wave rectifier, which has a maximum theoretical efficiency of 40.6%, or the full wave rectifier (FWR), which can improve the efficiency to 81% with a small increase in complexity. The efficiency of each of these devices can be calculated by dividing the DC Power delivered to a resistive load by the AC power that would have been delivered to the same load, had the source not been rectified. The rectifier's conversion efficiency can be obtained from the following equations,

$$\text{Efficiency} = \eta = \frac{P_{dc}}{P_{ac}} \quad (6)$$

$$P_{dc} = \frac{V_{dc}^2}{R} \quad (7)$$

$$P_{ac} = \frac{V_{rms}^2}{R} \quad (8)$$

$$P_{dc} = \frac{1}{\pi} \int_0^{\pi} V_p \sin(\theta) d\theta \quad (9)$$

$$P_{rms} = \left[ \frac{1}{\pi} \int_0^{\pi} V_p^2 \sin^2(\theta) d\theta \right]^{1/2} \quad (10)$$

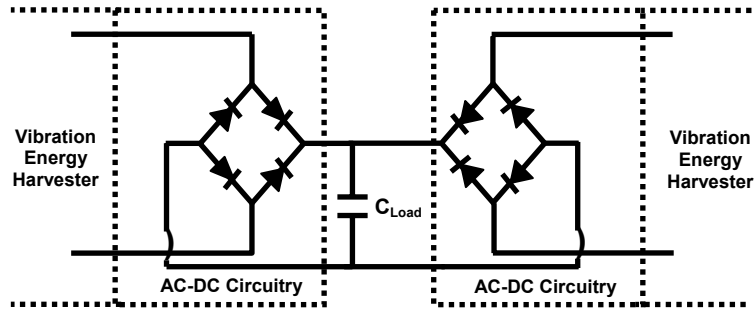


Figure 11. Energy Management Circuitry; Conversion to DC Signal with Dual Full-Wave Rectifiers

It is proposed that a further increase in performance in comparison to the basic full-wave rectifier is possible by combining two rectification circuits back to back and attaching two power harvesting sources to either end as shown in Figure (11). The advantage of this approach, apart from the simplicity of implementation, is that the independent sources may be viewed as a virtual multi-phase source. This yields a larger average voltage ( $V_{dc}$ ) as well as a higher  $P_{dc}/P_{rms}$  and therefore can deliver more power to the load than a single generator could, and at greater efficiency. Figure (12) illustrates the output voltage of the multi-phase rectifier.

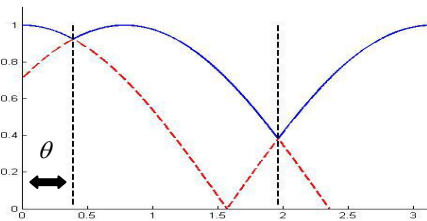


Figure 12. Calculation of the RMS and Average Voltage over  $\pi$  radians

The solid lines represent the signals over which RMS and average voltage are calculated. The interval is broken up into three separate regions and integrated for  $P_{rms}$  and  $P_{dc}$ . The solution for  $V_{DC}$  takes the form,

$$V_{DC} = \frac{V_p}{\pi} \left[ \sin\left(\frac{\theta}{2}\right) + \sin\left(\frac{\pi - \theta}{2}\right) - \sin\left(\frac{-\theta}{2}\right) - \sin\left(\frac{\theta - \pi}{2}\right) \right] \quad (11)$$

The multi-phase rectifier approach achieves efficiencies comparable to the combined outputs of individual rectifiers for each power source. The primary advantage is that without this approach, a separate DC-DC converter circuit must be connected to each FWR output. Using separate DC-DC converters for each source, while straightforward, can become prohibitive for systems with many power pickup points. The multiphase rectifier avoids the additional DC-DC converter stages, but it comes at a cost. The amplitude and phase angle of each connected source must be considered. Figure (13)

shows the impact of phase angle on the power delivered to a simple resistive load from two generators whose phase angles differ by  $\theta$ . Increasing the phase angle to 90 degrees decreases the DC value to its minimum. The plot is generated with a PSpice simulation using generator models with parameters close to that of the P-E system. The real power delivered by the two power harvester sources and dissipated by the resistive load is shown in the solid line. The dashed line represents the power dissipation in the load if one of the generators is removed, i.e. no phase dependence. Notice that the power delivered is nearly double that of the single generator case over a significant portion of the curve. However, it is also significantly less than double over other portions. It would make no sense from a power-transfer standpoint to use this arrangement if the expected phase difference of the sources would lead to lower power transfer than two individual sources combined at a later point in the power system. Figure (13) allows us to place a bound on the performance degradation. However, because the signal shown is periodic, the power output will be no worse than the lowest point on the curve. The implication of this plot is that the coupling between mechanical structures can be exploited for efficient power harvesting, but special care must be paid to the phase dependencies of the system.

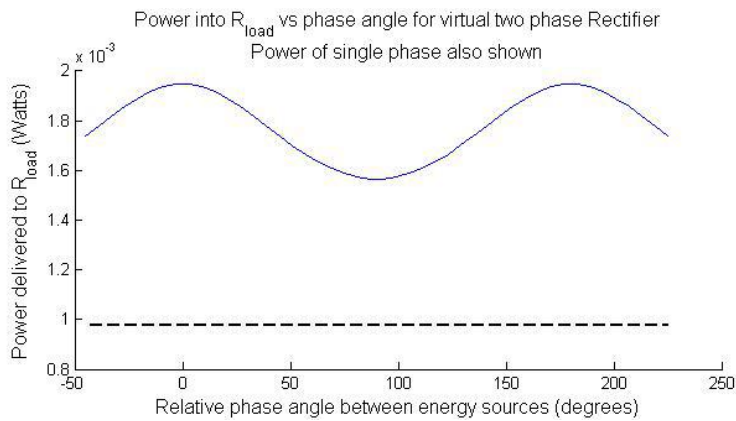


Figure 13. Dual-Full Wave vs. Independent Full-Wave Rectification

## 5. MAXIMUM POWER TRANSFER TO CAPACITIVE ENERGY STORAGE

The simplest model for the piezoelectric generator consists of an ideal voltage source in series with a capacitor. For the electromagnetic generator, the model is an inductor in series with a voltage source. These models are completely interchangeable with their Norton/Thevenin equivalent circuits by simply interchanging the parallel component for a series component or vice versa. The current or voltage must be scaled to ensure that the power output stays consistent,

$$V = I|X| \quad (12)$$

$$X_L = j\omega L \quad (13)$$

$$X_C = \frac{1}{j\omega C} \quad (14)$$

The optimal load for such systems consists of a complex impedance that exactly cancels the reactive impedance of the source. This however is not practical for the low operating frequencies typical of most power harvesting applications. For instance, a properly tuned inductor matched to cancel a 12nF source capacitance, typical of a small piezoelectric, would require 52kH of inductance! Therefore, a reactively matched approach is not appropriate. In order to achieve DC power delivery to the load, an impedance transforming circuit is required. The source has a relatively low AC impedance,  $X_C = -j*331k\Omega$ , but its DC impedance is infinite; the series capacitor blocks DC. A rectifier circuit transforms the infinite DC impedance to the lower impedance of its series, or parallel, component. Figure (14) shows the power dissipated by a resistive load connected to the output of a full wave rectifier. The power is maximized at a particular load, 331k $\Omega$ , which corresponds to the magnitude of the complex impedance,  $X_C$  of  $C_P$ .

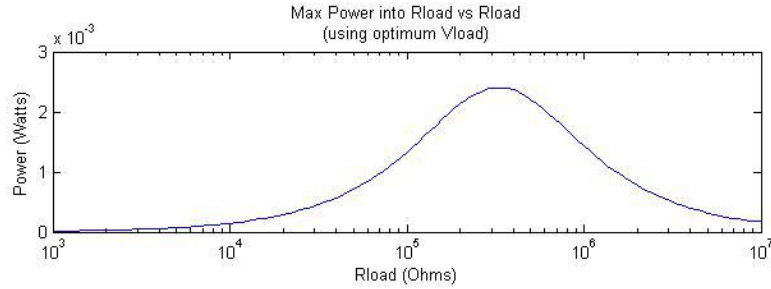


Figure 14. Piezoelectric Power into Resistive Load from Full-Wave Rectifier

While the resistive case illustrates the need for proper output matching, it is rare that a purely resistive load is placed at the output of the rectifier. An output capacitor,  $C_{Load}$ , is required in order for stored energy to be available at times other than when the harvester is generating electrical power. Figures (15) and (16) show the variable rate of energy delivery to the storage capacitor during the charging cycle by showing the power transfer from a full-wave rectified harvester to a capacitor as a function of time and voltage. The peak power delivery to the capacitor occurs within a band of voltages, centered at one half the open-circuit voltage of the harvester, in this case 20V. Diverging away from this point, either by discharging the capacitor to a load or charging the capacitor from the harvester, reduces the rate of power accumulation from the source. This shift does not affect the circuit's ability to draw power from the capacitor though. The conclusion from this finding is that in order to charge the capacitor as rapidly as possible, the system needs to maintain the operation of the capacitor as close to the half-open-circuit voltage point as possible. If  $V_{Cload}$  were to fall below this band, less power would be available to the load, and less overall power could be extracted from the vibration source. Correlating the slope of the energy plot in Figure (15) as  $V_C$  approaches zero volts with the slope of the power plot, it is observed that over a second of excitation is required to reach the maximum power transfer point. In order to reduce simulation time, a small capacitor was used. In practice, though, a much larger capacitor would be required to store sufficient charge for operation. The size of the output capacitor,  $C_{Load}$ , has an impact on output power if the generator's intrinsic capacitance,  $C_p$ , is greater than  $C_{Load}/100$ . As long as  $C_{Load}$  is above this limit, its size has no impact on power transfer, see Roundy et al. [5]. If  $C_{Load}$  is made arbitrarily large however, the time constant  $\tau_C=RC$  grows excessively large.

$$\Delta E = \frac{1}{2} C (V_i^2 - V_f^2) \quad (15)$$

To prove this point, assume that the electronics that the power supply supports contain a small radio that turns on for 10ms and consumes 50mW. This transaction depletes 495 $\mu$ J from the capacitor. If the capacitor started out at 5V and ends at 3V, the required capacitance is 60 $\mu$ F. This value corresponds to a  $\tau_C$  of 20.4s. When  $\tau_C$  is this large, the capacitor spends a great deal of time returning to the higher power transfer regime, see Figures (15-17).

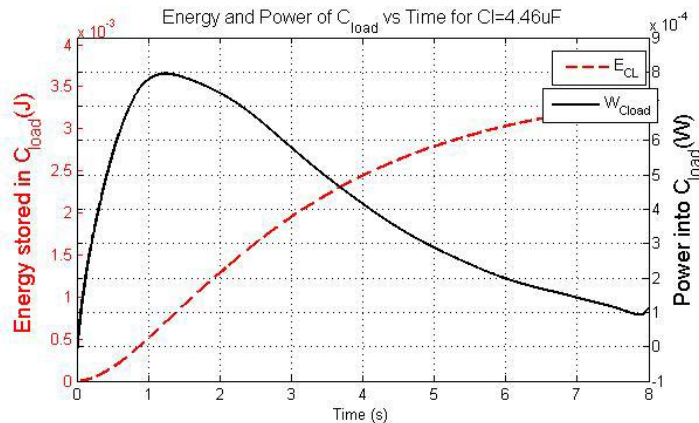


Figure 15. Piezoelectric Energy and Power Delivered by FWR into a 4.46 $\mu$ F Capacitor vs. Time

Figure (16) shows a potential control strategy for maintaining the capacitor voltage at the optimal point. The system controller monitors  $V_{Cload}$  and allows the voltage to climb to a setpoint, and then transfers energy out of the capacitor,

reducing  $V_{\text{Cload}}$  to a lower voltage on its operating curve. The system then disconnects from  $C_{\text{load}}$ , allows it to charge to the setpoint and the cycle continues.

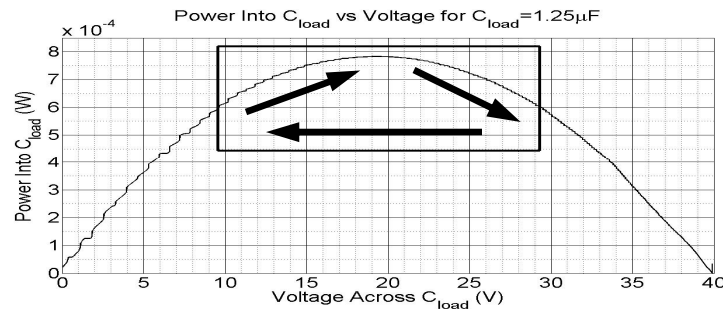


Figure 16. Power vs. Voltage for Piezoelectric Generator Model

While the electromagnetic generator model differs from the piezoelectric model, from a control viewpoint, their system performance, when rectified, is actually quite similar, compare Figure (16) and Figure(17). Each can be modeled as a simple RC circuit, with  $\tau_{\text{RC}}=RC$ . R is the magnitude of the source impedance and C is the rectifier output capacitance.

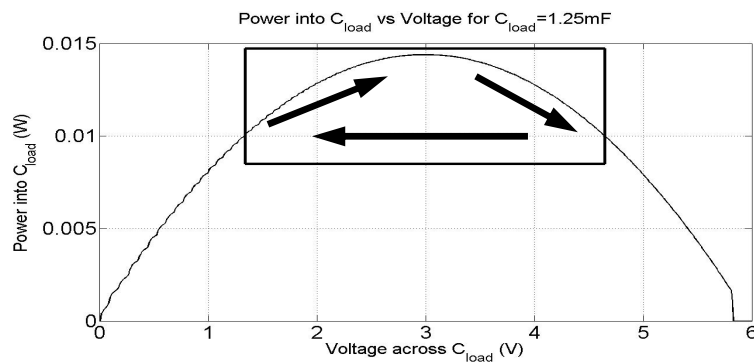


Figure 17. Power vs. Voltage for Electromagnetic Generator Model

## 6. DISCUSSION OF THE ENERGY STORAGE ELEMENT

### 6.1 Decoupling $C_{\text{Load}}$ From the System

The full-wave rectifier converts a high-impedance AC source to a high-impedance DC source, but the electronics in an autonomous, remote system often need a low-impedance source in order to transmit data, write to flash, or perform some other relatively power-intensive task. If the energy management system were implemented with only a very large  $C_{\text{load}}$ , with no additional storage or supervisory circuitry, the power-consuming systems would eventually discharge the capacitor well below its optimal power transfer band, and the system would be forced to gather energy at a lower rate until it moved back into the advantageous band. Several groups such as Chao et al. [20], Ottman et al.[11], Guyomar et al.[10] have decoupled the power harvesting electronics from the rest of the system by employing a DC-DC converter to transfer energy from  $C_{\text{Load}}$  to a much larger capacitor or battery. This allows  $C_{\text{Load}}$  to be relatively small, and respond to changes in excitation or reach an optimal power transfer state rapidly after long periods of inactivity. The optimal operating voltage for maximum power transfer is  $V_{\text{OC}}/2$ , however  $V_{\text{OC}}$  changes, depending on the excitation magnitude. The power management system monitors the excitation amplitude by measuring the voltage output of the source, or by measuring the current being delivered to  $C_{\text{Load}}$ , and transfers power to the much larger power storage element when necessary to maintain  $C_{\text{Load}}$  at an optimal level. This approach has the disadvantage of suffering additional loss due to the DC-DC buck converter, but techniques are available which enable conversion efficiencies near 90%, see Chao et al. [20] and Chen [21].

## 6.2 Storage Type Selection

Thus far we have discussed  $C_{Load}$ , which is the relatively small capacitive load,  $1\mu\text{F} - 100\mu\text{F}$ , directly attached to the FWR. Large capacity storage has not been explicitly specified. Apart from self-winding watch mechanisms which store energy in a spring, few mechanical techniques exist that efficiently harness and store micropower signals. More options exist in electrical storage but with caveats. Guan and Liao [22] compared a commercially available supercapacitor, a Lithium Polymer battery and a NiMH battery. They investigated charge/discharge efficiency as a function of charge/discharge current as well as lifetime. The measured efficiency of the supercapacitors was higher than that of the LiPo or NiMH cells but was still relatively low at 66%. A hypothesis is that this may have been due to the intrinsic leakage current in supercapacitors. Typical values of leakage current for supercapacitors in the 1-5F range are 50uA to 1.5mA. There is wide variation in published specifications, but the leakage current generally scales with capacitance, as it is a function of the capacitor's surface area. This constant current can overwhelm the power harvesting capability and become a net drain on the system if not recognized and accounted for. Lithium batteries have much lower self discharge than supercapacitors, and their energy densities are typically an order of magnitude better than supercapacitors, but they do suffer a greater charge/discharge efficiency penalty than supercapacitors. They also have a vastly reduced cycle lifetime, relative to supercapacitors. Essentially, there is no right answer for system-level power storage. The solution must be tailored to the application. In situations where high power availability is likely, i.e. a great deal of vibration on a consistent basis, a supercapacitor-based design allows a practical number of charge/discharge cycles. The relatively higher self discharge is accommodated by the higher power availability. In a circumstance with infrequent, low level vibrations, a battery based solution would enable a very low power system to maintain a "sleep" current for a longer period of time than would a supercapacitor based solution.

## 7. CONCLUSIONS

Much of the power harvesting literature has focused on areas such as modeling of the transducer types and optimizing the power transfer for single type energy harvesters, i.e. piezoelectric harvesters. This paper adds to the literature by exploring the effects of the relative phases of the transduced electrical energy using a multi-component power harvesting system, in which piezoelectric and electromagnetic harvesters are attached to a vibrating structure. The analysis presents an electromechanical dynamics model that determines the relative phases of the coupled piezoelectric and electromagnetic harvesters for varying driving frequencies. Each of these harvesters are then modeled using PSpice to assess the maximum power transfer prior to and after rectification. Schemes are proposed for simple, direct combination of sources and the implications are assessed. Lastly, a discussion is presented for selection of the energy storage element based on specific design goals.

## ACKNOWLEDGMENTS

This work is supported by the Microsystems Technology Office.

## REFERENCES

- [1] Sodano, H. A., Inman, D. J., and Park, G., "Generation and storage of electricity from power harvesting devices," *J. of Intelligent Material Systems and Structures* 16(1), 67-75 (2005).
- [2] Glynne-Jones, P., Todor, M. J., Beeby, S. P., and White, N. M., "An electromagnetic, vibration-powered generator for intelligent sensor systems," *Sensors and Actuators* 110, 344-349 (2004).
- [3] Fleurial, J. P., Snyder, G. J., Herman, J. A., Smart, M., Shakkottai, P., Giauque, P. H., and Nicolet, M. A., "Miniaturized thermoelectric power sources," *Proc. SAE IECEC*, 992569 (1999).
- [4] Raghunathan, V., Kansal, A., Hsu, J., Friedman, J., and Srivastava, M., "Design considerations for solar energy harvesting wireless embedded systems," *Proc. ISIPSN*, 457-462 (2005).
- [5] Roundy, S., Wright, P. K., and Rabaey, J. M., [Energy Scavenging for Wireless Sensor Networks], Kluwer Academic Publishers, Boston / Dordrecht / New York / London, 167-175 (2004).
- [6] Mateu, L., and Moll, F., "Review of energy harvesting techniques and applications for microelectronics," *Proc. SPIE* 5837, 359-373 (2005).

- [7] Goldfarb, M., and Jones, L. D., "On the efficiency of electric power generation with piezoelectric ceramic," *ASME J. of Dynamic Systems, Measurement, and Control* 121, 566-571 (1999).
- [8] Reissman, T., Dietl, J. M., and Garcia, E., "Modeling and experimental verification of geometry effects on piezoelectric energy harvesters," *Proc. IEEE ISAF*, EH024 (2008).
- [9] Pereyma, M., "Overview of the modern state of the vibration energy harvesting devices," *Proc. IEEE MEMSTECH*, 107-112 (2007).
- [10] Guyomar, D., Richard, C., Lefeuvre, E., and Petit, L., "Piezoelectric non-linear systems for standalone vibration control and energy reclamation," *Proc. Adaptronics Congress* (2004).
- [11] Ottman, G. K., Hofmann, H. F., and Lesieutre, G. A., "Optimized piezoelectric energy harvesting circuit using step-down converter in discontinuous conduction mode," *IEEE Transactions on Power Electronics* 18(2), 696-703 (2003).
- [12] Shu, Y. C., Lien, I. C., and Wu, W. J., "An improved analysis of the SSHI interface in piezoelectric energy harvesting," *J. Smart Materials and Structures* 16, 2253-2264 (2007).
- [13] Roundy, S. and Wright, P. K., "A piezoelectric vibration based generator for wireless electronics," *J. Smart Materials and Structures* 13, 1131-1142 (2004).
- [14] Poulin, G., Sarraute, E., and Costa, F., "Generation of electrical energy for portable devices; comparative study of an electromagnetic and a piezoelectric system," *Sensors and Actuators* 116, 461-471 (2004).
- [15] Khattak, A. R., Garvey, S. D., and Popov, A. A., "Repeated resonances in folded-back beam structures," *J. Sound and Vibration* 290, 309-320 (2006)
- [16] Shu, Y. C. and Lien, I. C., "Analysis of power output for piezoelectric energy harvesting systems," *J. Smart Materials and Structures* 15, 1499-1512 (2006).
- [17] Sodano, H. A., Park, G., and Inman, D. J., "Estimation of electric charge output for piezoelectric energy harvesting," *J. Strain* 40, 49-58 (2004).
- [18] Greenhouse, H.M., "Design of planar rectangular microelectronic inductors," *IEEE Trans. Parts, Hybrids, and Packaging* 10(2), 101-109 (1974)
- [19] Reissman, T., Park, J. S., and Garcia, E., "Microsolenoid electromagnetic power harvesting for vibrating systems," *Proc. SPIE* 6928, 6928-9 (2008)
- [20] Chao, L., Tsui, C.Y., and Ki, W.H., "Vibration energy scavenging and management for ultra low power applications," *Proc. IEEE ISLPED* (2007)
- [21] Chen, J., "Determine buck converter efficiency in PFM mode," *Proc. IEEE Power Electronics Technology*, 28-33 (2007)
- [22] Guan, M., and Liao, W., "On the energy storage devices in piezoelectric energy harvesting," *Proc. SPIE* 6169, (2006)